Available online at www.sciencedirect.com
SCIENCE DIRECT
Catalysis Today 114 (2006) 126–141
CATALYSIS TODAY
www.elsevier.com/locate/cattod

Towards designing pillared clays for catalysis

A. De Stefanis, A.A.G. Tomlinson *

Istituto per lo Studio dei Materiali Nanostrutturati, Area Ricerca C.N.R., C.P.10 Monterotondo Staz., 00016 Rome, Italy

Available online 28 February 2006

Abstract

Recent advances in tailoring pillared clays (PILCs) for catalytic applications are reviewed. Emphasis is placed on the variety of reactions beyond acid catalysis: cracking, dehydrogenations, oxidations and particularly clean technology applications, especially De–NO_x, which can be carried out in PILCs. Further, recent structure determinations via SANS (small angle neutron scattering) methods have allowed, for the first time, determination of inter-pillar distances, permitting construction of pore geometries. This has also been found possible for the related restructured clays and the SANS-determined structures of K10 and Mg-HMO are reported. The latter is the first of a new type of mildly restructured montmorillonites important in industrially relevant alkenylation reactions for producing key organic intermediates. Implications of these recent advances for eventually designing PILCs for specific catalytic applications are discussed.

Keywords: Pillared clays; Catalyst design; SANS structures

Clays have a long and chequered history in industrial sorption and catalysis, which for some time has veered towards possible clean technology applications [1]. They are also still of interest catalytically, given the absence of a single detailed reaction mechanism for organic reactions on their surfaces. For both pillared clays (PILCs) and restructured clays (i.e. clays in which the layer structure has been partially destroyed by acid treatment) the major reason is the absence of detailed structures. We recall, for example, that the structure of montmorillonite itself is essentially an extrapolation of that for mica, determined over 60 years ago. Nevertheless, the nineties saw a boom in both materials characterisation and catalytic work on PILCs [2], which has been much reviewed [3]. Instead, this overview has the more modest aim of underlining the versatility of PILCs as catalytic supports and emphasizing salient problems remaining in the field with pointers as to how current materials tailoring could move into real catalyst design.

PILCs are traditionally formed via insertion of a poly-hydroxy-metal species into a smectite clay, followed by calcination of the flocculated product to give materials in which a nano-oxide moiety props apart the layers. The interlayer is opened out making large surfaces available for chemical reactions, as shown in Fig. 1. Major alternative preparations widening the tailoring options are also shown, up to the more recent direct insertion of nano-oxide particles of differing dimensions. Also included is a speculative PILC structure in which the pillar now consists of other platelets; this may provide a means of covering the (inactive) surface of an active catalyst (say, MoS_2) making more of the (active) edge available.

The major characteristics of the materials obtained are well known. Porous solids can be obtained possessing S/V ratios so high as to allow accessible internal surfaces of $>800\ m^2\ g^{-1}$, according to some authors. In general, PILCs obtained through route 1 usually possess accessible internal surfaces of 150–$450\ m^2\ g^{-1}$. Secondly, the materials are micro-texturally complex although geometrically constrained. This textural complexity is due to a combination of many factors: interlayer distance distribution, deformation (bending) of host (which can lead to myriad types of edge–edge, face-edge, etc., platelet associations). In turn, the micro-texture is very sensitive to details of the wet (or colloid) chemistry involved, the drying methods adopted and details of calcinations conditions. The sum total is that the materials generated are supermesh structures, the complexity of which explains why there have been few advances to date in understanding catalytic properties.

The large S/V ratios are usually adduced as being the major reason for catalytic interest in PILCs. Instead, perhaps a more fundamental reason is that having porous structures where an oxide and an aluminosilicate are (almost...) perpendicular to

* Corresponding author.
E-mail address: gus@mlib.cnr.it (A.A.G. Tomlinson).

0920-5861/$ – see front matter © 2006 Elsevier B.V. All rights reserved.
doi:10.1016/j.cattod.2006.01.019

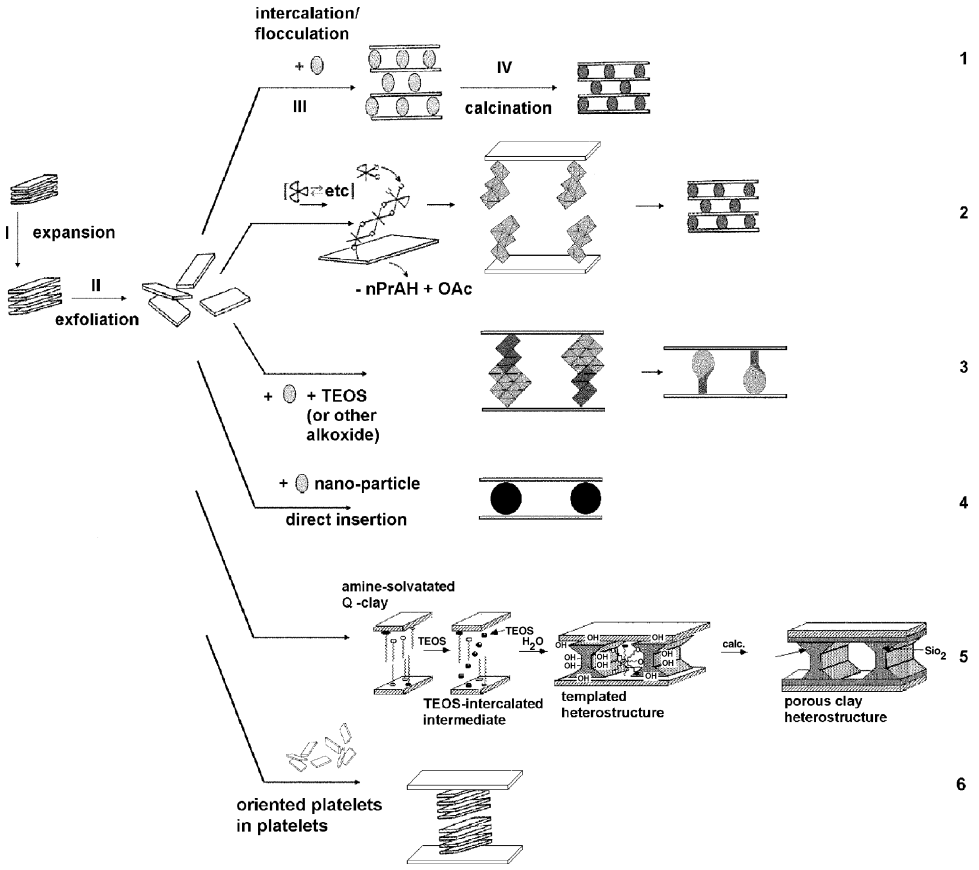

Fig. 1. Current methods for pillaring clays. 1. Traditional route, using Al_{13} Keggin ion for alumina pillars, etc; 2 [4]; 2. A surface hydrolysis/polymerisation reaction, used for preparing chromia-pillared PLS [5], 3. Via sol–gel generated intercalates, both homogeneous and heterogeneous (that shown) [6]. 4. Direct intercalation of externally generated known-size nano-particles (including surface derivatised analogues) [7]. 5. Assisting interpillar spacing via amines and surfactants [8]. 6. An example of possible use of platelets themselves as pillars.

one another will give rise to highly anisotropic pores. This is shown in Fig. 2 and clearly, the potential exists for manipulating the pore electrostatic energies so that they lie within the ranges for bond-breaking and bond-formation for specific organic reactions.

Further, this anisotropy in pore electrostatics should also increase for transition metal exchanged PILCs, to reach a maximum for PILCs having differing types of layers, such as interlayered clay/phosphates for example. These exist [10] but have not yet been pillared.

Returning to Fig. 1, going from pore tailoring to design has been stymied over the years because most work on route 1 was (and is) carried out on local clays, and is still centred on montmorillonites. Because deposits of these regularly have both interlayer (especially Fe and Cu, but also Li) and surface (both transition metal and Ca in particular) substitutions, this introduces systemic non-reproducibility in final materials. Interlayer substitution particularly influences the precursor intercalation phase (III), which involves precursor particle/colloid–dispersed layer interactions, in turn depending on concentration of each component, pH, temperature, rheological properties, and washing or other clean-up methods, such as dialysis.

Intercalant distributions will then differ (through, for example, ion migration, coordination at impurity sites, etc.) which is exacerbated at higher concentrations because of increase in particle agglomeration, with increase in nano-species present (Fig. 3). The variety of polycrystalline and/or amorphous end-products after the least controllable step, i.e. calcination, then vitiates attempts to rationally position nano-oxides, even for the alternative routes. Indeed, the figure actually underestimates the characterisation problems because pore blocking (e.g., by fragments generated during pillaring if some clay layer restructuring also occurs) and incomplete pillaring must also be taken into account.

Nevertheless, despite these well-documented colloid chemistry and characterisation problems [11], over the past fifteen years considerable effort has been devoted to the standardisation of procedures as to produce industrial quantities of alumina montmorillonite PILCs. To date this is the case for AZA, FAZA, the particularly clean EFW, a purer Bohemian smectite (IKO-Erbslöh, Germany) and the non-montmorillonite-contaminated beidellite B4 (S&B, Greece) of more recent interest to us, together with other cleaner montmorillonites: CW (Ca-white) and NNB, from the same suppliers. By concentration control and minimisation of washing volumes, a scale-up quality alumina-EFW could be obtained and the cleanest possible (given its provenance from deposits containing both montmorillonitics and beidellitics) B4 analogue. For EFW, reproducible scale-up was achieved using much-reduced

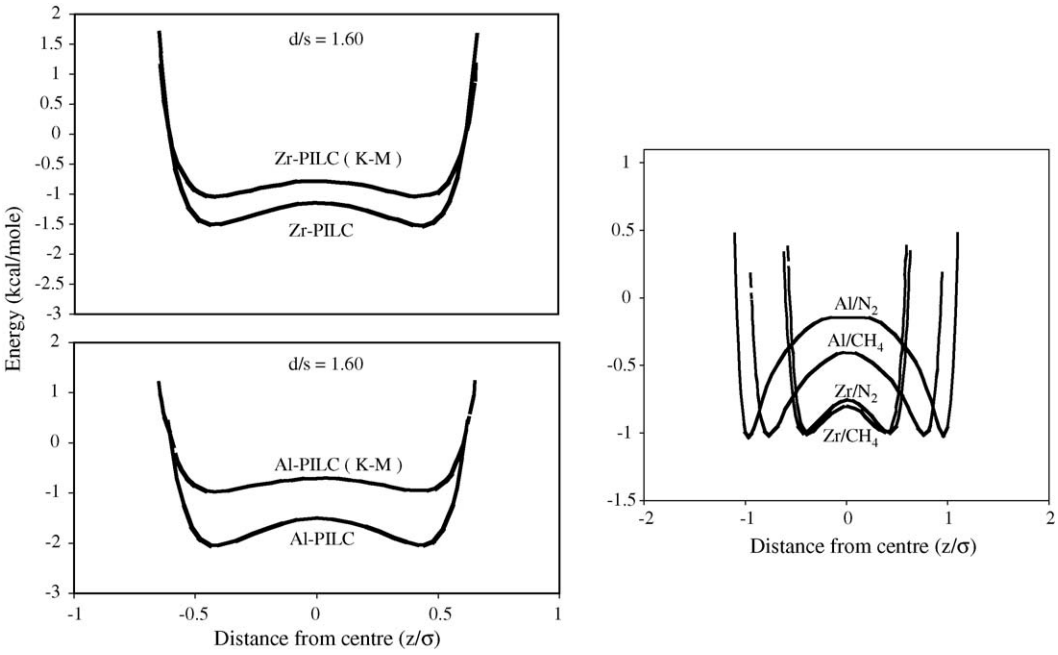

Fig. 2. Potential energy profiles of Zr- and Al-PILCs for a given pore size ($d/\sigma = 1.60$) (left) using the Kirkwood–Muller formalism; for N_2 and CH_4 using the same methods [9].

quantities of water [12]. The large quantities of water necessary for clean-up (20 L per 1 g) is a factor overlooked in laboratory studies, and the relevant results are shown in Table 1.

Throughout, standard BET N_2 sorption/desorption isotherms provide a measure of materials quality control, as shown in Fig. 4.

Nevertheless, the structural characterisation problems consequent on the effects shown in Fig. 3 remain, as can be seen in the XRPD of these Al-EFWs and the structurally related (yet of very different sorption/catalysis) beidellites (Fig. 5). XRPD provide mainly information on interlayer distance alone, as discussed in detail previously [12].

However, the most serious problem remains quantitation of porosity. The standard BET treatment of N_2 sorption/desorption is based on the 'herringbone' array of N_2 molecules sorbed on a surface (Fig. 6).

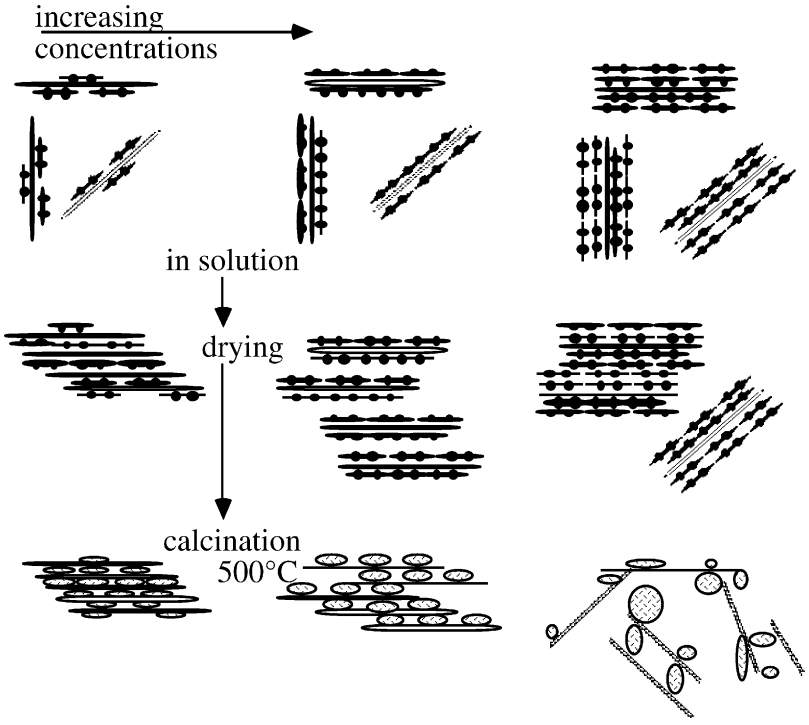

Fig. 3. Influence of concentration on final materials textures during the process [11].

Table 1
Illustrating the effect of washing-water volume in scale-up of preparation of Al-EFW

Amount of water decreased (ml)	Concentration, (g/l) (bentonite of pillaring system)	Specific surface area (m^2/g)	Specific pore volume (μl/g)	Specific micropore volume (μl/g)
950	9.1	236	190	115
1950	14.3	309	235	140

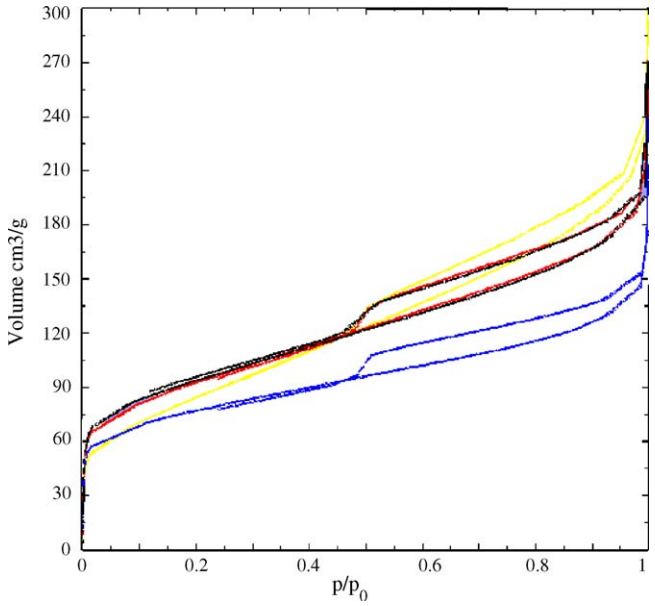

Fig. 4. N_2 adsorption/desorption isotherms of Al-pillared EFW montmorillonite clays. Black = lab-scale pillared clays with 3.0 mmol Al/g bentonite; red = pillared clays of concentrated pillaring system (14.3 g/L); yellow = - pillared clays of up-scaling with OH/Al ratio 2.4; blue = pillared clays of up-scaling with OH/Al ratio 2.0. From top: pillared clays of up scaling with OH/Al ratio 2:4; lab scale pillared clays with 3.0 mmol Al/g bentonite; superimposed: pillared clays of concentrated pillaring system (14.3 g/L); pillared clays of up scaling with OH/Al ratio 2.0.

In turn, the BET equation is based on calculation of space requirements from properties of three-dimensional condensed N_2 phases *via*:

$$\alpha = f(M/\rho N)^{2/3} (\alpha = \text{area of} N_2 \text{ molecule})$$

p is the density of 3D reference phase, M the mol.wt., N the Avogadro No.

Originally (EB) α was calculated from liq. N_2 density

$$f = 1.0911 \quad \alpha(N_2) = 16.2\,\text{Å}^2$$

Many years ago [13], a careful SPM investigation demonstrated that in reality the 'footprint' of N_2 at a surface is modified by the electric field which couples with the quadrupole moment. The effect tilts the molecule away from being strictly // to the surface and although the degree of tilting is small, it is sufficient to give rise to modified $\alpha(N_2) = 13.5\,\text{Å}^2$, which in turn affects the PSDs by overestimating the importance of micropores in the slit-pore, cylindrical-pore and other models used.

This has been known for some time and workers have used various methods of sorption/desorption curve interpretation (αs, *ts* methods, etc) to correct for it [14]. The most appropriate for PILCs appears to be those developed for a slit-pore model by Vansant et al. in the early nineties [15]. The first, the mean pore (MP) method, requires low-pressure measurements and calculates mean group pore sizes directly from the average value for two points on a *t*-plot. Pore volume (at a point) is obtained from extrapolation to the adsorption axis, and the average size of micropores can be derived. However, corrections must be applied for irregular pore shapes, i.e. poor estimated pore sizes and these are not easily applicable. A subsequently 'modified MP method' utilising multi-step *t*-plots and not requiring low-pressure apparatus, was found to be more amenable to correction [16]. The method derives external surface areas and specific micropore volumes via *t*-plot and αs-plot methods by comparison with a non-porous reference. Details of plot analysis are given in the references; in summary,

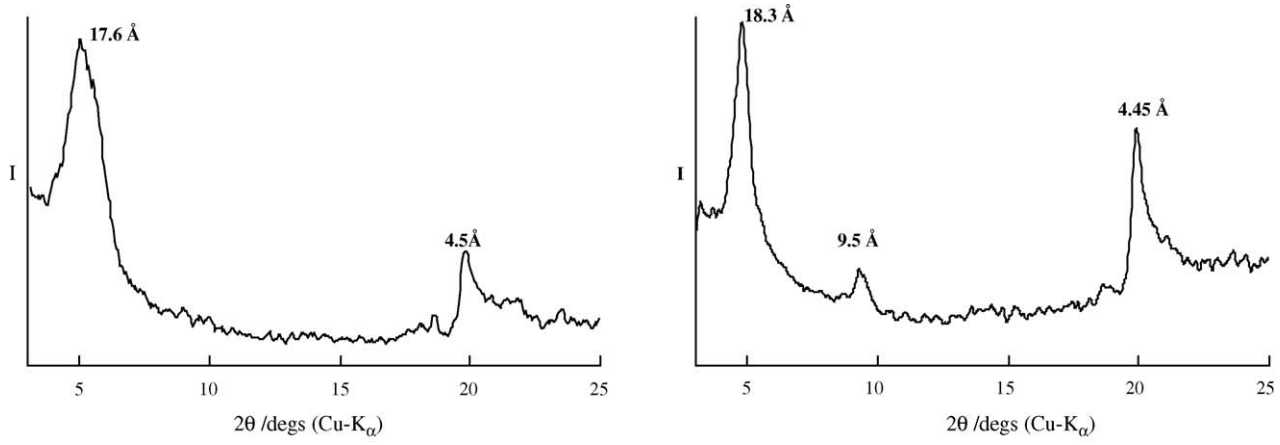

Fig. 5. XRPD of Al-EFW (left) and Al-B4 (right).

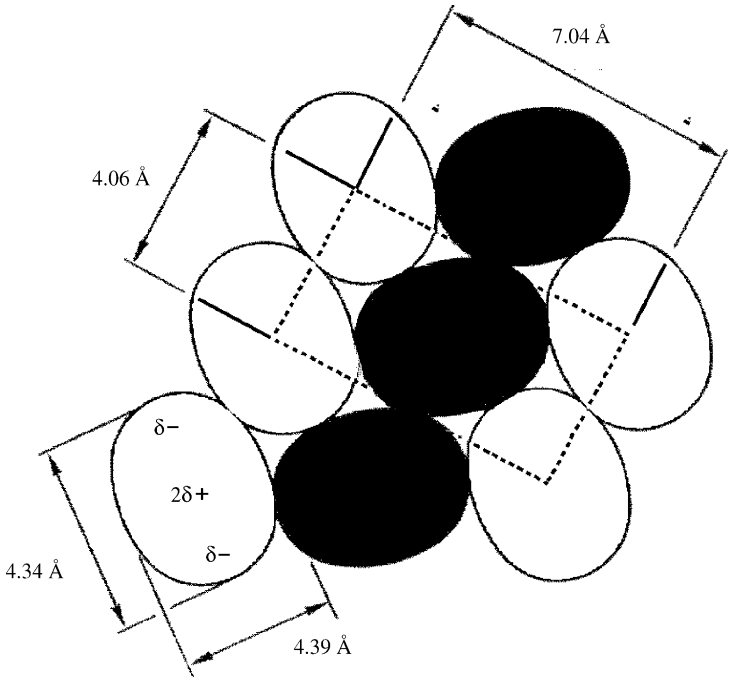

Fig. 6. Herringbone arrangement of N_2 molecules on a surface.

the surface area of a group of pores of similar pore size is obtained from slope differences at tangents drawn at two adjacent points. As an example, Fig. 7 shows PSDs for several new alumina-PILCs discussed here, together with changes resulting after cation exchange [17]. Such PSDs allow coverage of pores by cation to be estimated, and – eventually – should permit conclusions to be drawn on which pore is responsible for catalytic reaction.

In parallel with these developments, in the early nineties standard materials were made available via the Concerted European Action on Pillared Layered Structures ('CEA-PLS', referred to in [1]) in an attempt to eliminate systematic materials differences deriving from differing processing and characterisation methods. Three materials were made available, two: AZA and FAZA -$(Al_2O_5)_n$- pillared Greek "Zenith-N" bentonites of formulae:

AZA : $(Na_{0.62}K_{0.25}Ca_{0.013})\,[Si_{7.75}Al_{0.25}]$
$(Al_{3.41}Mg_{0.48}Fe_{0.05}{}^{3+}Ti_{0.07})O_{22}\,nH_2O$

FAZA : $(Na_{0.08}K_{0.26}Ca_{0.06})[Si_{7.75}Al_{0.25}]$
$(Al_{3.38}Mg_{0.55}Fe_{0.05}{}^{3+}Ti_{0.02})O_{22}\,n'H_2O$
$+\,(0.24Fe_2O_3 + 0.58Al_2O_3)$

The third, ATOS was an alumina-pillared saponite, derived from a TOLSA (Spain) saponite.

(FAZA is believed from Mossbauer measurements to have a pancake pillar: 1 nm high × 9.5 (±2.5) nm diameter, containing well-dispersed Fe^{2+} and Fe^{3+}).

At that time, our interests also included the alumina PILCs:

- FAZN: a non-commercial analogue of FAZA, prepared under more controlled conditions.
- BP-PILC: –$(Al_2O_5)_n$–/montmorillonites, as used by BP in an industrial process (see below).

Porous alumina-pillared Group IV phosphates, and Cr^{3+}-pillared analogues (CrZrP) with BET N_2 surfaces ranging from 120 to 250 $m^2\,g^{-1}$ (former) to 250–400 $m^2\,g^{-1}$ (latter) [5].

A considerable body of sorption/catalysis results was accumulated, the latter ranging from alcohol conversions, dehydrogenation, alkylation, and the staple conversions of early zeolite chemistry, including fluidised catalytic cracking (f.c.c.). However, during the course of that work, it was discovered that rather than being mineralogically pure montmorillonites, Greek "Zenith-N" bentonites in reality are mixed montmorillonite/beidellites [18]. It was previously thought that there were no beidellite deposits in Europe. This does not vitiate the catalytic results, most of which were at the scoping level, comparing yields, selectivities, etc., i.e., following gross effects of surface area, pore size reactivity and which reactions occur at pillar and which at sheet. We subsequently extended these *via* comparison with those for commercial zeolites. Table 2 lists early probe reactions utilised in the project; methods used, i.e. static (vials) or dynamic (modified pyrolysis reactor, fixed-bed, etc.) and conditions may be found in the individual references.

1. Alcohol dehydration/dehydrogenation

Alcohol conversions provide the simplest and clearest example of reactivity modulation *via* pillaring. Parent cation-exchanged: Cu-saponite, -montmorillonite, etc., convert MeOH to mainly methyl formate and formic acid, Conversely, on PILCs MeOH is converted to dimethylether (DME) in high yield. Single- and double-cation exchange lead to large reactivity changes; Ni-FAZA and K-Ni-FAZA (i.e. Ni-FAZA

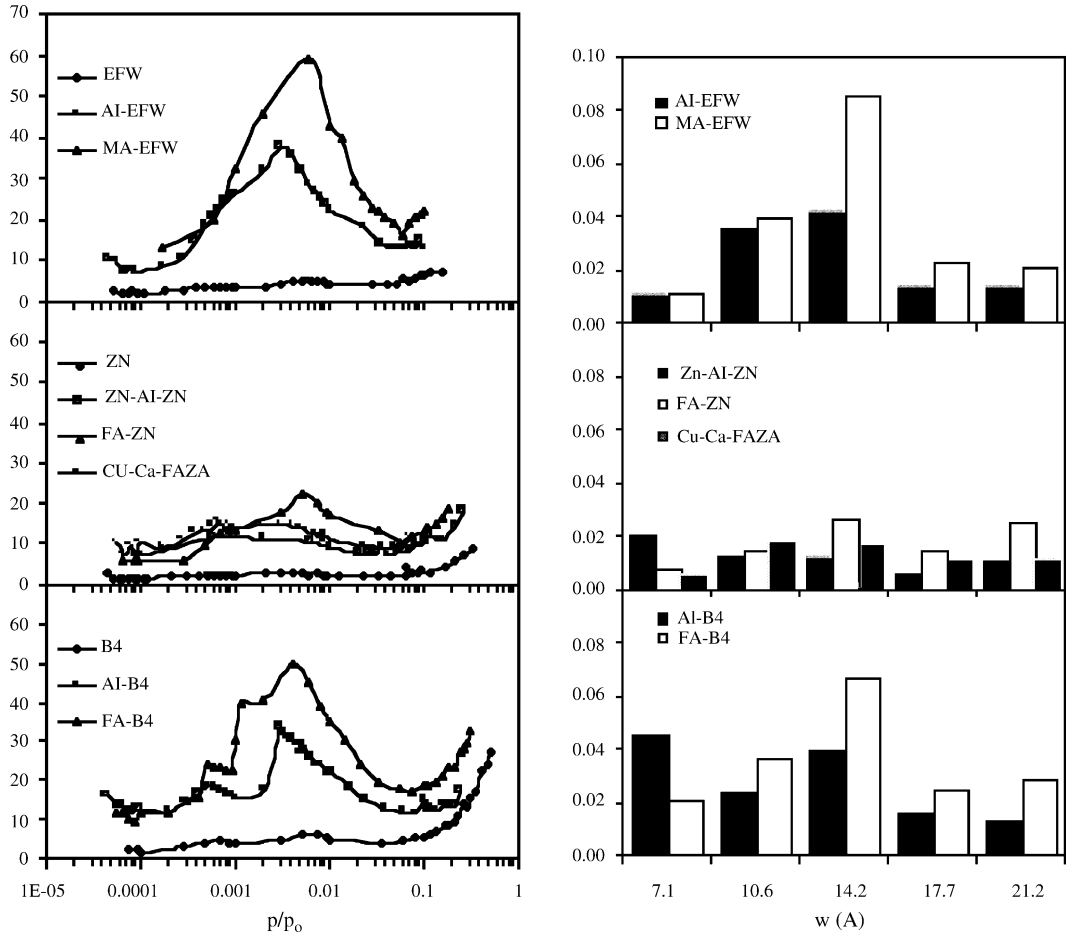

Fig. 7. Pore size distributions for several new PILCs and changes caused by cation-exchange, as derived from the Modified MP method [*x*].

subsequently exchanged with K+) suppress DME production in favour of mixed hydrocarbons whereas the opposite occurs in Cu–Ca–FAZA [19]. The large changes are ascribed both to steric effects and to selective blocking of proton-containing active sites. Presumably, highly acidic Lewis active sites are generated on Ni^{2+}-exchange of FAZA and it is interesting that the hydrocarbons distribution is similar to that obtained in the MTG process. Although a catalytic probing exercise, such reactions may also be of use: DME is an unlikely fuel (it is a gas) but the related ethylmethyl ether is a possible fuel and suitable modified PILCs would be of interest.

Turning to EtOH, overall conversions lie in the order:

BP-PILC > AZA > FAZA = ATOS

whereas ethane/acetaldehyde ratios in the order:

BP-PILC > FAZA > AZA > ATOS

Although all are less active than ZSM-5 zeolite, both orders point to BP-PILC as being the most Lewis acidic. However, to complicate this picture, dehydration occurs by two pathways; the first giving ethane *via* a monomolecular mechanism (and probably involving surface alkoxy groups), the second leading to diethyl ether (DE). The latter is important only <300 °C and occurs by bimolecular elimination and these product outcomes is given by zeolites but not by smectite clays themselves. It was concluded that reaction mechanisms and reactive sites for AZA and BP-PILC are similar and the latter are at the sheets. For the first reaction, changes in dehydrogenation/dehydration ratio with flow rates instead point to the presence of two differently sized pores.

The systematics prompted us to suggest that the crossover point between the two reactions with temperature variations (shown in inset in Fig. 8, and termed the iso-acidic point) represents the point at which Lewis and Brönsted acidity are

Table 2
Catalytic probe reactions for PILCs vs. zeolites

Reaction	Materials	Objectives
Alcohol dehydration/dehydrogenation	Metal substituted Al and Al/Fe pillared clays	Brönsted/Lewis *iso*-acidic point
Ethylbenzene to styrene	K-FAZA	Dehydrogenation vs. dealkylation
p-Xylene methyl alkylation	Restructured clays	Influence of pore size on bimolecular reactions

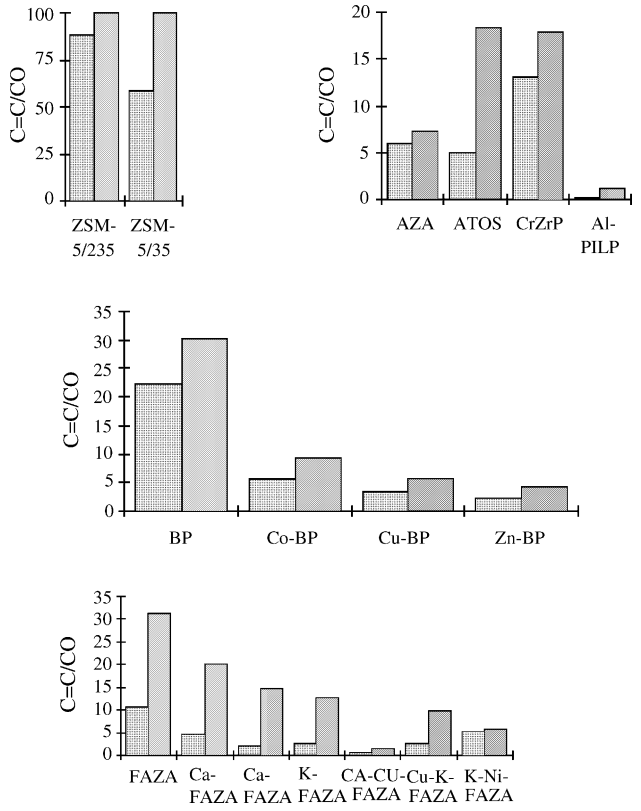

Fig. 8. C=C/CO ratio at 600 °C for ethanol (▨) and *iso*-propanol (▩).

the same strength. This could be used to construct an acidity scale for PILCs and other porous materials [19].

Finally, it was concluded that the Brönsted site generating the intermediates for dehydrogenation is 1 rather than 2 (Scheme 1).

2. Ethylbenzene to styrene [20]

The second probe reaction, not given by zeolites, is the dehydrogenation of ethylbenzene (EB), also an important petrochemical process (the Badger process) (Scheme 2):

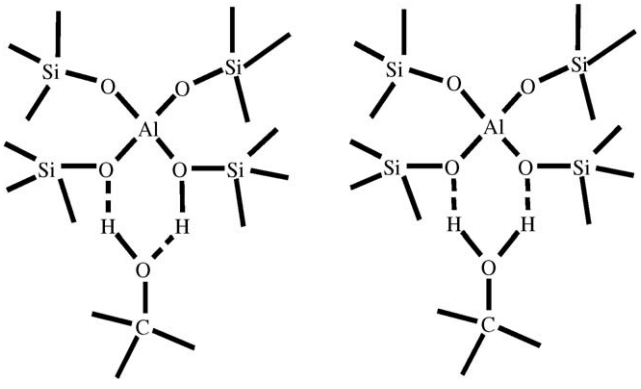

1 2

Scheme 1.

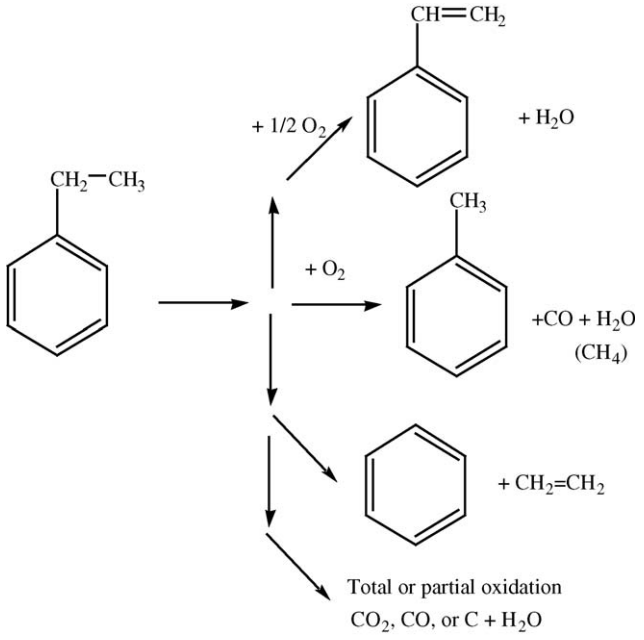

Scheme 2.

Conversions of ethylbenzene both to diethylbenzenes (EB → DEB) and to styrene (EB → Styr) were investigated on AZA- and FAZA-derived PILCs. In EB → DEB conversion, the PILCs give higher conversion than do ZSM-5s ($SiO_2/AlO_2 = 35$ and 235) and other mid-pore zeolites, with a comparable selectivity towards *p*-DEB. Detailed comparisons of catalytic properties suggest the PILCs contain specific pore exit channels - or dimensions similar to those found in ZSM-5 zeolites - rather than a random supermesh structure and differ from mid-pore zeolites in acting more as acidic reaction vessels. Conversely, the shape-selectivity characteristics of ZSM-5s depend on pore access/exit modes. This implies that during the shape-selective bimolecular reaction, sorbate molecular orientation is controlled by electrostatic anisotropy between aluminosilicate layer and oxide pillar.

Although PILCs are active in EB → Styr conversion non-selectively and only at high temperatures (>450 °C), they become much more active and highly selective over a wide temperature range (between 100 and 600 °C) after metal-cation exchange. Beidellitic-PILCs are more active and selective than montmorillonite-PILCs and those containing mixed $Fe^{2+}Fe^{3+}/Al^{3+}$ pillars (e.g., FAZA) more than those with unsubstituted alumina pillars. Conversion yields for FAZA lie in the order:

$$Ni^{2+} > Co^{2+} > Cu^{2+}$$

and Ni^{2+}-FAZA is the most unfavoured as regards disproportionation to benzene (2.5% at 450 °C). Although Cu^{2+}-FAZA gives low conversions (<12% at 500 °C) it shows the highest selectivity (100%) for styrene (Fig. 9).

The high activity and selectivity for K^+-FAZA suggest – as also put forward for commercial α-Fe_2O_3 catalysts - that $KFeO_2$ might be formed at the alumina pillar (Fig. 10).

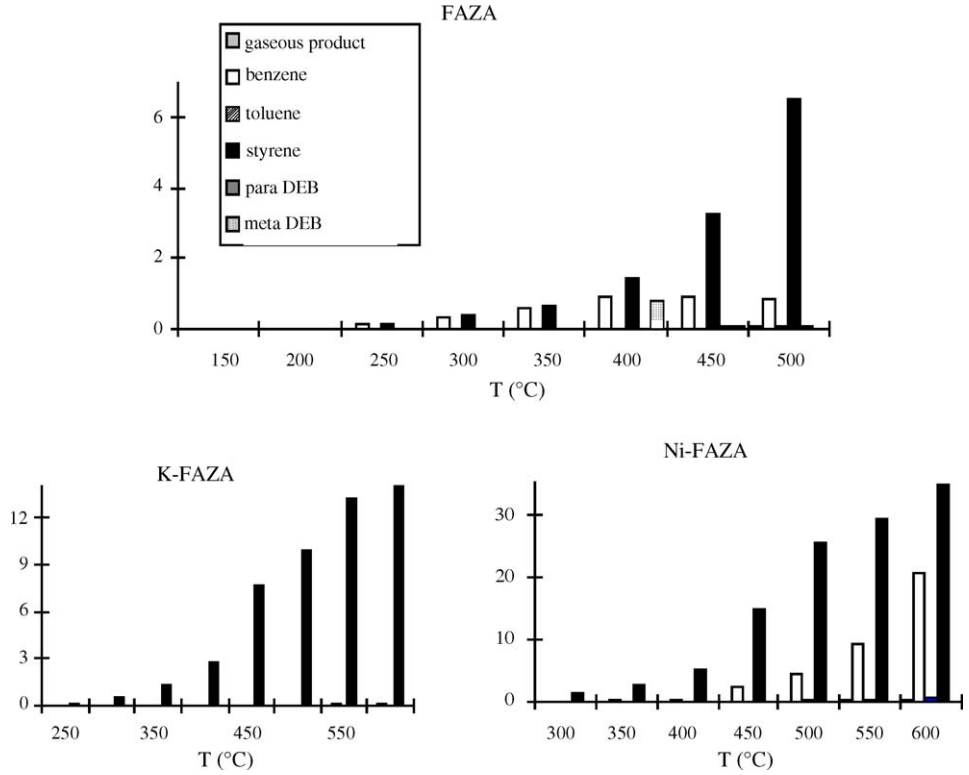

Fig. 9. Styrene yields on FAZA and K-, Ni-exchanged analogues.

Finally, the more bulky alkylbenzenes, *n*-PrB, *n*-BuB, etc, do not undergo dehydrogenation on all the catalysts tested, so the reaction can also be performed in their presence.

3. Aryl alkylations

Also instructive as regards comparing pore sizes in PILCs with those in zeolites are benzene alkylation reactions, which may be summarised as Scheme 3

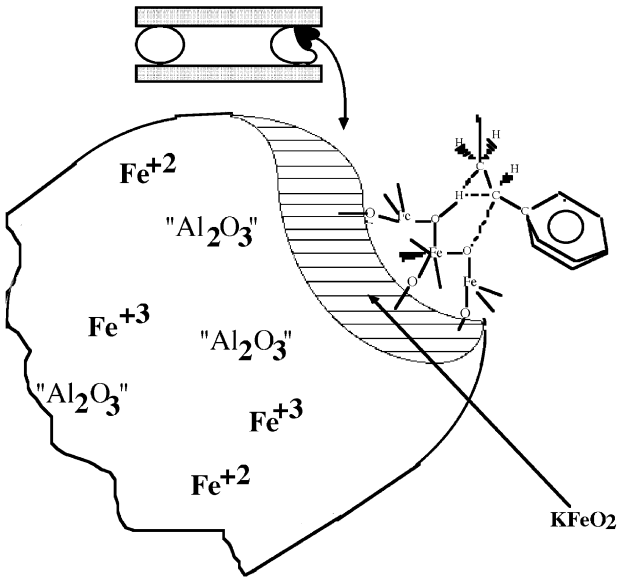

Fig. 10. Suggested active site in FAZA, showing possible intermediate.

The alkylation of benzene by MeOH, EtOH, iso-PrOH and *n*-octanol has been investigated in ZSM-5, mordenite, USY and Theta-1 and the acidity/porosity relations obtained compared with those in an alumina-pillared montmorillonite (BP-PILC) and an alumina-pillared saponite (ATOS) [21]. For MeOH, pseudo-first order alkylation rates follow the order:

ZSM-5 > mordenite > USY > Theta-1 > ATOS > BP-PILC

which for the zeolites is not that expected on the basis of acidity. Conversely, EtOH conversions in ZSM-5s with Si/Al ratios 5/35 → 5/400 do follow expected acidity trends and MeOH destruction can be used to construct an acidity scale.

It is concluded that the pore size is the determining factor, i.e., it is crucial in modulating the electrophilic attack of intermediate matrix-attached oxonium ion at incoming benzene molecules. Rather than a consequence of low acidity, it appears that it is the too large pore sizes of both PILCs which hinder efficient alkylation as shown convincingly in Fig. 11.

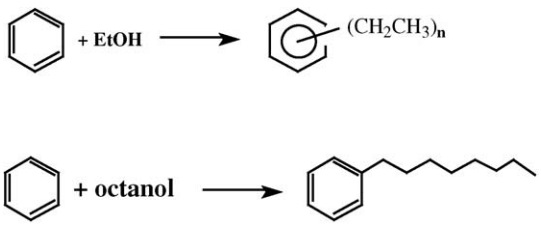

Scheme 3.

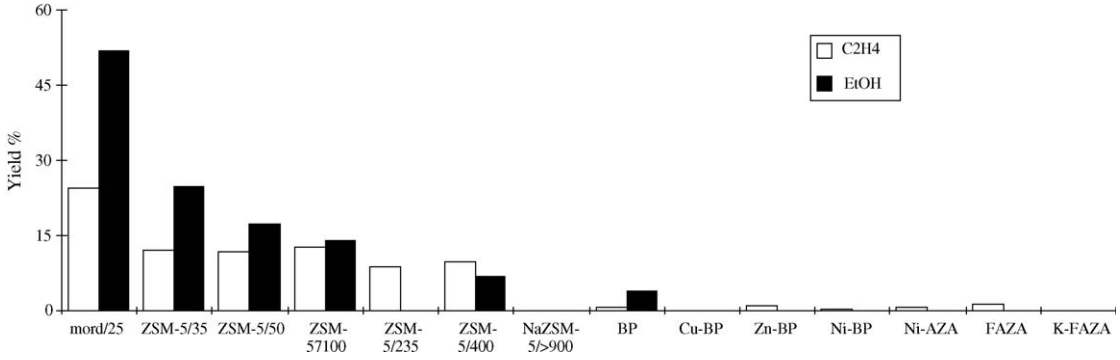

Fig. 11. Yields of alkylation products of reaction of benzene with ethene and EtOH on several zeolites and PILCs.

4. Industrially important reactions

Originally, the highest hope for PILCs was as substitutes for f.c.c. catalysts, currently based on zeolite Y and ZSM-5 formulations capable of withstanding the super-heated steam temperatures (680–720 °C) necessary for catalyst regeneration (Fig. 12):

The intention was to substitute the zeolite component(s) withPILCs having pore sizes large enough to crack organics with diameters > ca 8 Å (the limit for f.c.c. zeolites) whilst at the same time robust enough to withstand steam regeneration [22,1]. Particular attention was paid to pillared rectorites; rectorite is a Stage II clay related to illite and micas, a fact suggesting added stability. Although this does indeed appear to be the case, rectorite deposits are rare (only in China and in insufficient amounts to be economically viable). From the recent advances outlined here and elsewhere, especially in the availability of synthetic clays [4] we suggest that more fruitful would be investigations of pillared synthetic micas.

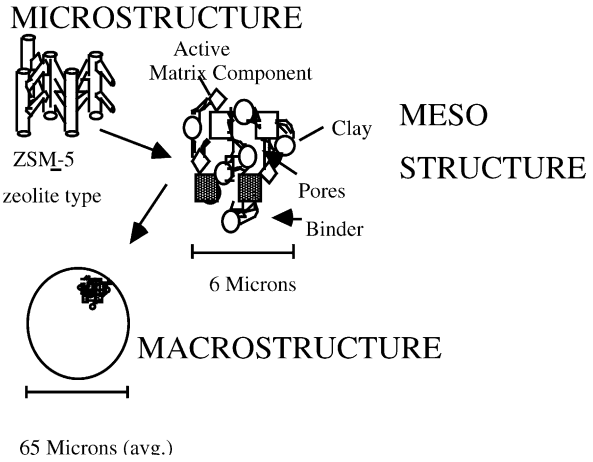

Fig. 12. A typical f.c.c. catalyst formulation.

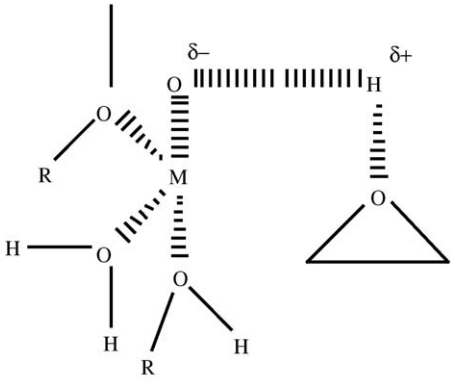

Scheme 5.

5. Glycol ether production [23]

Attention subsequently shifted to bulk chemicals, as exemplified by the BP process – of some 20 years ago – for glycol ether (as used in anti-freeze formulations) production from ethene oxide (EO) and EtOH (Scheme 4):

The activities are shown in Fig. 13 which shows that the proton exchanged BP-PILCs are the most active and this depends also on preparation method:

H^+-PILC via H^+ layered clay exchanged with $[Al_{13}]^{7+}$
> H^+-PILC via NH_4^+ exchanged alumina pillared PILC
> H^+-PILC calcined parent alumina pillared PILC

Metal-exchange causes large activity decrease, the bulky non-polarising cations (Cs^+) being virtually inactive. Further, a possible active site was suggested (Scheme 5) which, however, seems to apply to metal-ion centres alone.

The subsequent advances discussed below should allow this mechanism to be placed on a more secure basis.

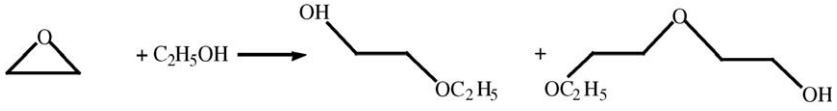

Scheme 4.

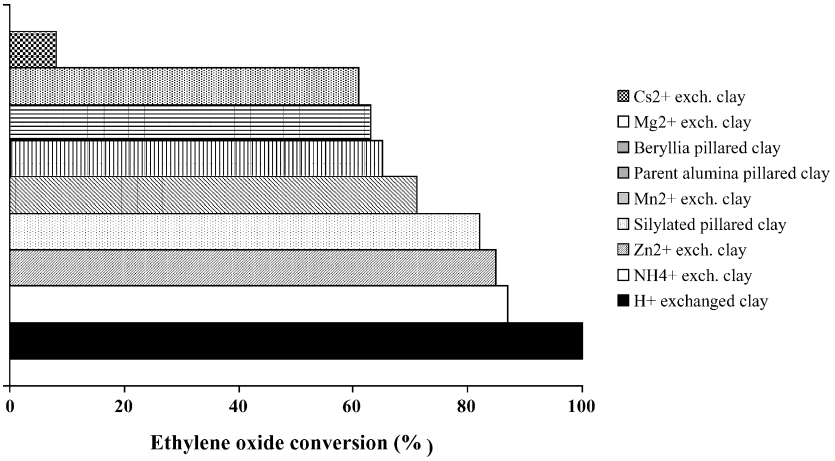

Fig. 13. Activities of alumina-pillared BP-PILC derivatives in glycol ether production. Conditions: T 90–93 °C; P 22–26 bar; LHSV 0.25.

6. Propene oxide (PO) from *n*-propanol [24]

As shown by the probe reactions, possible utility is not solely in acid-catalysed reactions, however. During probing reactions, it was found that on many PILCs *n*-PrOH is converted to propene oxide (PO) (Scheme 6):

The reaction is carried out in the absence of oxygen (or H_2O_2) stream and Fig. 14 illustrates yet again how sensitive

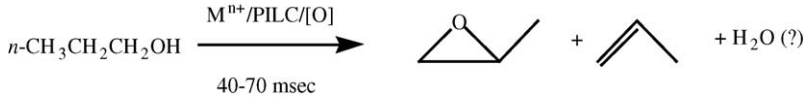

Scheme 6.

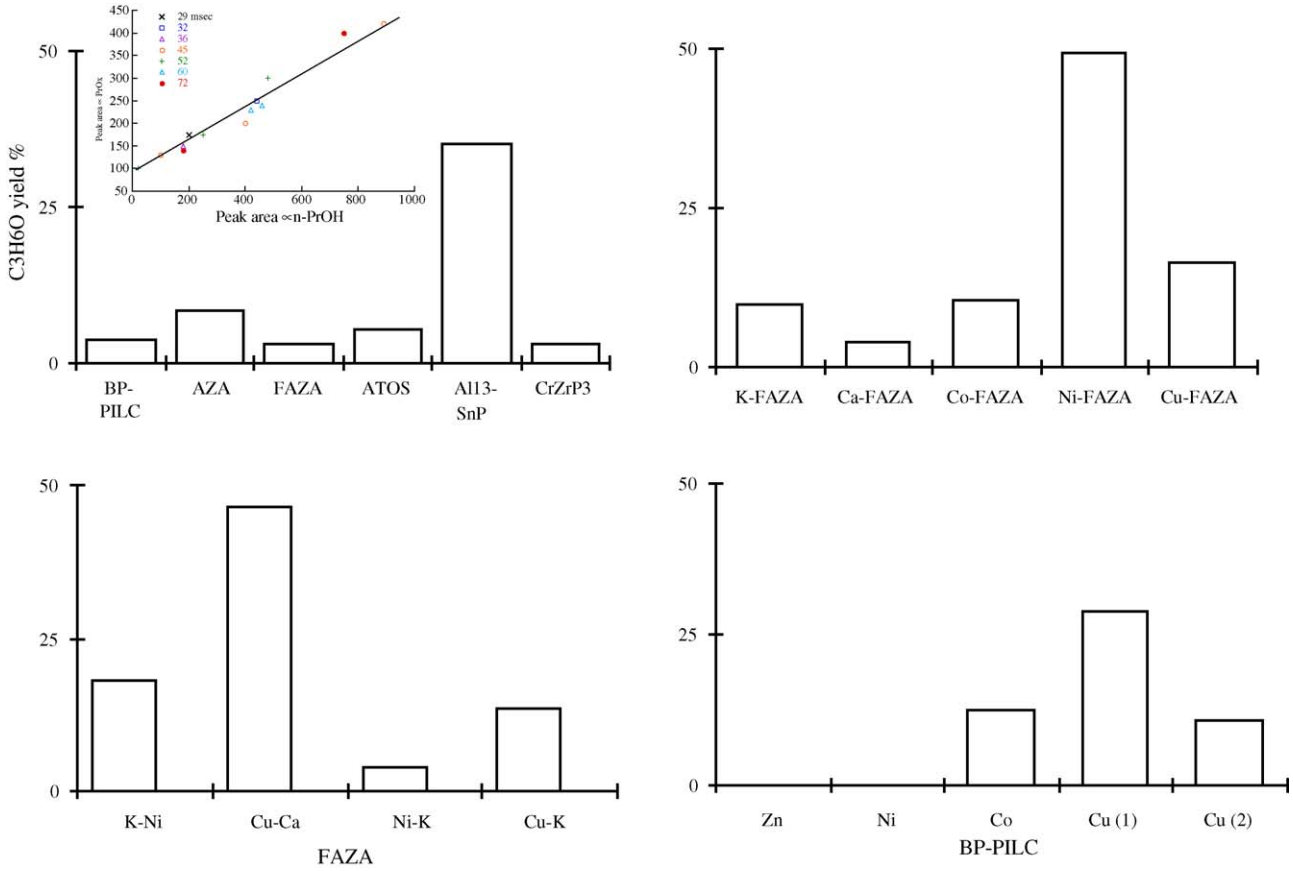

Fig. 14. Activity of various Al-PILCs and Al_{13}–SnP in PO production from *n*-PrOH.

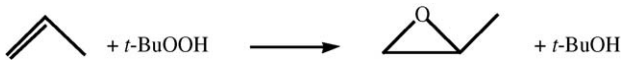

Scheme 7.

yields are to cation-exchange: note that CrZrP3, a chromia-pillared zirconium phosphate expected to be an oxidising agent, is not very active.

That Ni-FAZA is one of the most active is not surprising (see above) because a dehydrogenated intermediate is probably generated. Indeed, reactions must be carried out at contact times < 0.4 s to avoid propene production).

Currently, PO is produced mainly by ARCO technology, which is based on the stoichiometric reaction (Scheme 7):

Apart from being inefficient, this reaction involves labile, explosive and expensive *t*-BuOOH and designing catalytic systems to directly oxidize olefins to epoxides using oxygen and a co-reductant (H_2) has been a long-standing goal. This proposed new route on modified clays seems promising.

7. PILCs as 'reaction vessels'

To the variety of non-acid catalysed reactions of PILCs can also be added their utilisation as 'reaction vessels'. Again, the combination of pore anisotropy and cation exchange can lead to products very different than those found for zeolite 'reaction vessels' (long suggested as possibly useful industrially). A good example is CCl_4 which, unusually, is highly sorbed (retention: 100% at 450 °C by G.C.) on alumina PILCs and the intermediates generated used to activate benzene under both static and dynamic conditions [25]. Chlorobenzene (PhCl) and biphenyl are the main products (with benzoyl chloride the only other side-product, see Fig. 15). Overall yields of Al-montmorillonite PILCs as such are low (2–4%, calculated on starting benzene) but increase when a transition metal-containing pillar is present (e.g., FAZA, which has activity comparable with the mid-pore zeolite ZSM-5). Yields increase much further (e.g., PhCl $\gg$ 5%) when the Al-PILC is cation exchanged, as in Cu-FAZA.

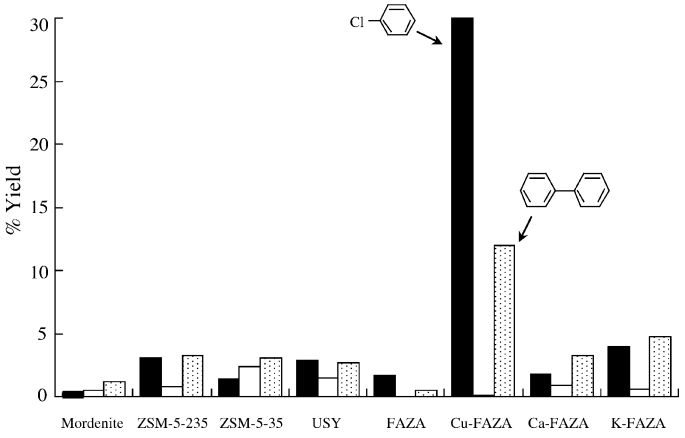

Fig. 15. Relative chlorobenzene and biphenyl yields from reaction of benzene with CCl_4 encapsulated in PILCs. Yields calculated with respect to CCl_4.

The strong inversion in chlorobenzene/biphenyl ratio (reflecting cation intermediate *via* free-radical mechanism ratio changes) is being investigated mechanistically.

8. De–NO_x reactions

Titania-pillared montmorillonites have long been known to be active in De–NO_x reactions [26] which increase expectations that PILCs may substitute some current catalysts in clean technology. This is especially so since the putative substitutes for the current V/TiO_2 catalysts for standing sources: CuZSM-5 and $Pt/\gamma\text{-}Al_2O_3$ have disadvantages. The former is de-activated by H_2O (CoZSM-5 more efficient) and although most resistive in the presence of H_2O and SO_2, and showing high selectivities for N_2O formation and $SO_2 \rightarrow SO_3$ oxidation, the latter has only a narrow operability window.

Taking N_2O abatement first, efficient conversions can be obtained on many Al-PILCs, with beidellite-based ones being more active than montmorillonites-based ones (as shown in the example of Fig. 16) [27]. The results indicate that the yield of the reaction ($N_2O \rightarrow N_2 + O_2$) increases when pillared clays are exchanged with transition metals, single-pass conversion rates of >70% being attainable. In particular, when double exchanged (calcium and subsequently copper) alumina pillared montmorillonite/beidellite is used as a catalyst, de–N_2O activity reaches a maximum, which is maintained even after 4 h of work at a space velocity of 5.5 h^{-1}.

On oxide catalysts, adsorption of N_2O is the first step of the reaction:

$$N_2O_{(gas)} \rightarrow N_2O_{(ads)} \quad (1)$$

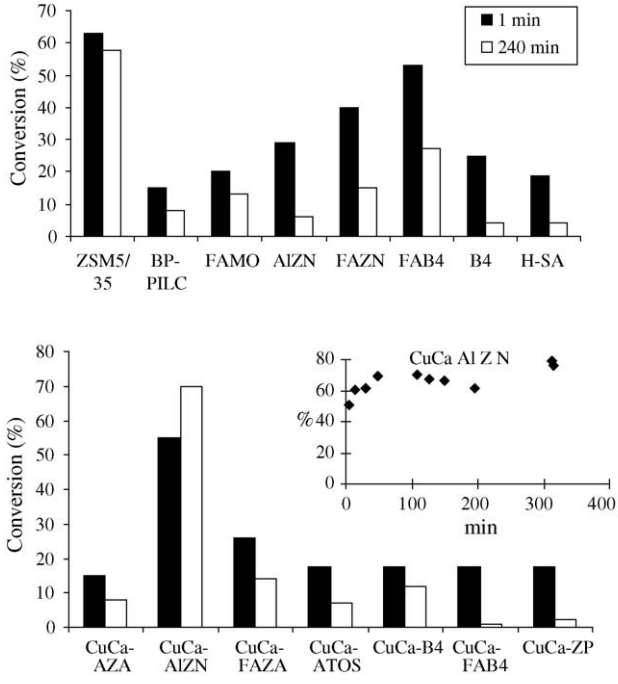

Fig. 16. N_2O abatement on various montmorillonites and beidellite-based PILCs in the presence of methane. Space velocity 5.5 h^{-1}. Inset shows conversion time course for the best catalyst. See [28] for materials.

After which, the adsorbed N_2O can undergo two reactions. The first implies an oxidation of the catalyst:

$$N_2O_{(ads)} \rightarrow N_{2(gas)} + O_{(ads)} \quad (2)$$

and the second a catalyst reduction:

$$N_2O_{(ads)} + O_{(ads)} \rightarrow N_{2(gas)} + O_{2(gas)} \quad (3)$$

The same overall mechanism applies to Al-PILCs series.

At the beginning of the reaction there is a deficiency of active oxygen in the catalyst and oxidation of catalyst is the main reaction; only later do both reactions concur in N_2O destruction. The presence of methane is important because it removes the oxygen via the reaction:

$$O_{2(gas)} \rightarrow 2O_{(ads)} \quad (4)$$

avoiding the oxidation of catalyst. The competition of such reactions with catalyst oxidation by N_2O can explain the effect of oxygen on the destruction of N_2O.

More recently it has been found that alumina-pillared laponites are even more efficient for both NO_x abatement [28]. Exchanged Al-laponites show extreme variations in yield and in selectivity, as illustrated in Fig. 17 again for the case of N_2O. Not only are activities higher than for aluminosilicate-based PILCs, but there are variations in activity when the pillar contains iron. N_2O abatement is halved for the Cu^{2+}-and V^{3+}-exchanged catalysts, but more than doubled for the Co^{2+} and Mn^{2+} analogue, for reactions on alumina-pillared laponite containing iron in the pillar. These variations strongly point to the active site(s) being located on the pillar and also, in the iron-containing pillar case, to the probable presence of binuclear metallic sites. However, the most important point is that the higher activity in general must also be connected to differences in sheet structure between montmorillonites and beidellites on the one hand and hectorite on the other.

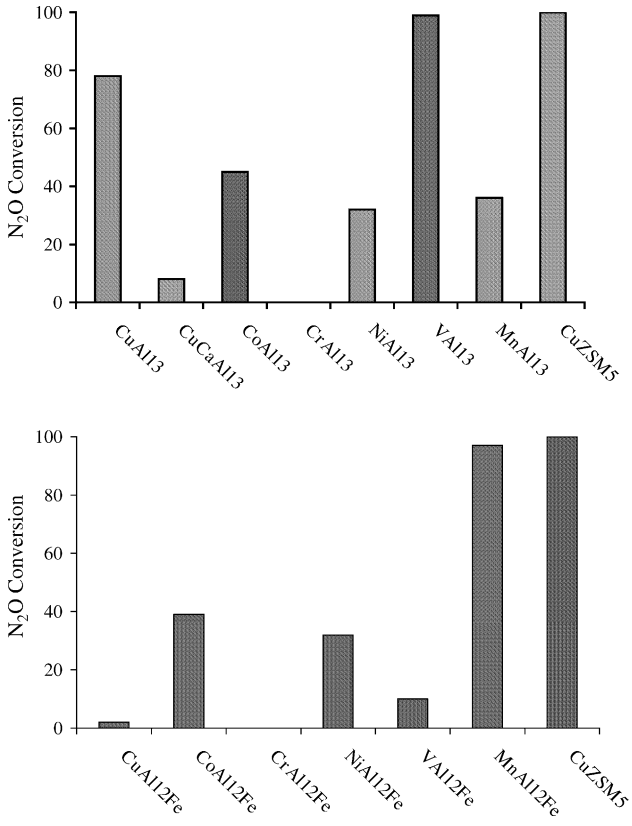

Fig. 17. N_2O abatement on transition metal exchanged alumina- and Fe-alumina pillared laponites in the presence of methane. Cu-ZSM-5 is shown for comparison.

Laponite is a synthetic hectorite; morphologically, it is of very small platelet size (and amorphous). Platelet edge structure is then more developed than platelet face structure and they are very different, i.e., activity differences may be connected with the presence of more active edge sites. Mechanistic studies are underway to clarify this suggestion. Whichever of these two effects turns out to be the more important after completion of detailed spectroscopic investigations, it appears that the V^{3+}-exchanged non-iron containing catalyst is a good candidate for replacing the current de-NO_x catalysts. In sum, PILC-based catalysts should take their place in replacement of current ammonia technology. Indeed, we recall that urea-based standing-source technology (developed as a substitute for the ammonia in current use) has recently been transferred to moving sources [29] and that other amines have also been proposed as ammonia substitutes. Consequently, one useful route would be to investigate use of in situ amine as reducing agent in the PILCs described above (and others with titania pillars).

9. Catalysts for LCO hydrotreating

Cracking and hydrotreating of LCO to high-cetane index (CI) fuels is an important petrochemical process, and the current trend is to partially hydrogenate the polyaromatics compounds to form aromatic naphthenic molecules which are then cracked to high CI alkylaromatic ones.

Current catalysts include supported Ni/Mo, Pt/Pd, Ir/Ru and others. Decalin and tetralin are probe molecules of choice because they indicate which catalyst is best for cracking or hydrotreating and also for probing the best pore/acidity character of catalysts [30].

Fig. 18 gives an overview of some results obtained from a set of Ni–Mo double-exchanged alumina-pillared montmorillonites of the EFW series (EFW, CW, etc.) mentioned above and compared with those for Ni-MCM41 and Pt-mordenite [31]. The most active are the saponite-based ones (ca. 30% of the saponites surface is beidellitic in nature) an indication that pore acidity is important. For mesoporous zeolites, conversions mainly depend on pore size, whereas in PILCs, access/pore size/acidity correlations are complex, as shown by Fig. 19 for tetralin. Conversions *increase* as surface areas *decrease*, possibly pointing to a single active pore among many. In conclusion, Ni- and Mo-based PILCs may be useful for substituting (or perhaps being used in conjunction with) current catalysts in light cycle oil (LCO) processing. Studies of access dynamics and metal ion geometries at Ni–Mo sites are currently underway to clarify the detailed mechanisms [31].

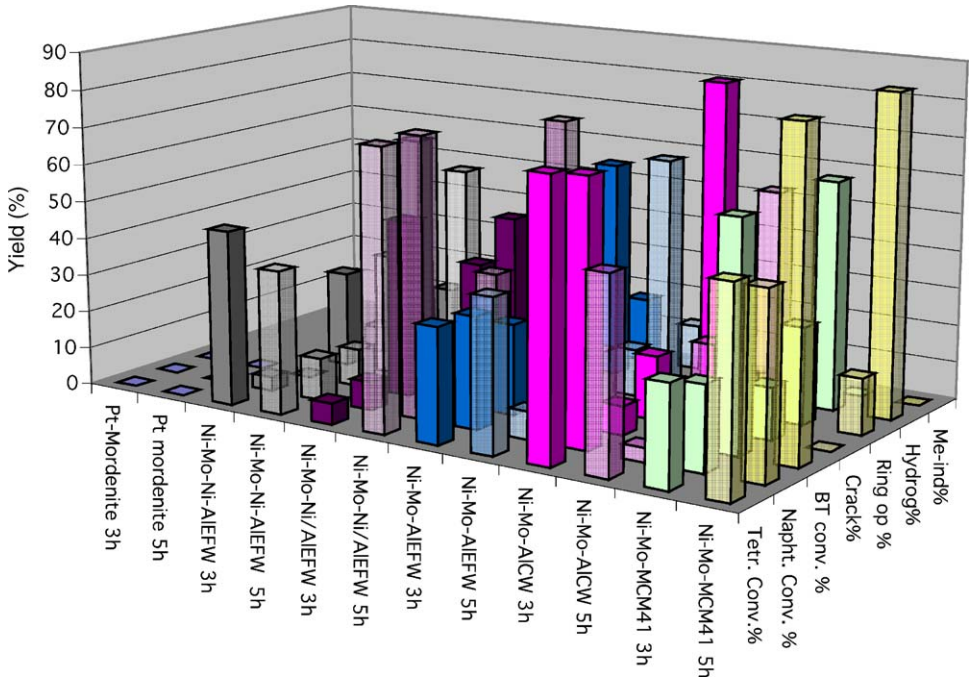

Fig. 18. Tetralin conversion with time on a Ni–Mo-PILCs series. Pt–mordenite and Ni–Mo MCM41 are shown for comparison.

10. The structure problem: SANS

To be able to place the above reactions on a more quantitative basis requires more structural data, which in the case of PILCs boils down to determining interpillar distances. We have had recourse to small angle neutron scattering (SANS) known to provide geometrical nanostructural (1–100 nm) information on porous materials. As for X-ray diffraction, SANS is a coherent scattering technique in which the scattered intensity $I(Q)$ is obtained from experimental measurements as a function of angle 2Θ, where $\Theta = 4\pi \sin \Theta/\lambda$. The neutron scattering length density, ρ, of a molecule of i atoms is then readily calculated from:

$$\rho = \Sigma_i b_i \mathrm{d}NA/M_\mathrm{w}$$

where b_i is the scattering length of the individual atoms in the molecule, the bulk density of the scattering object, M_w is its molecular weight and NA is the Avogadro number. Since

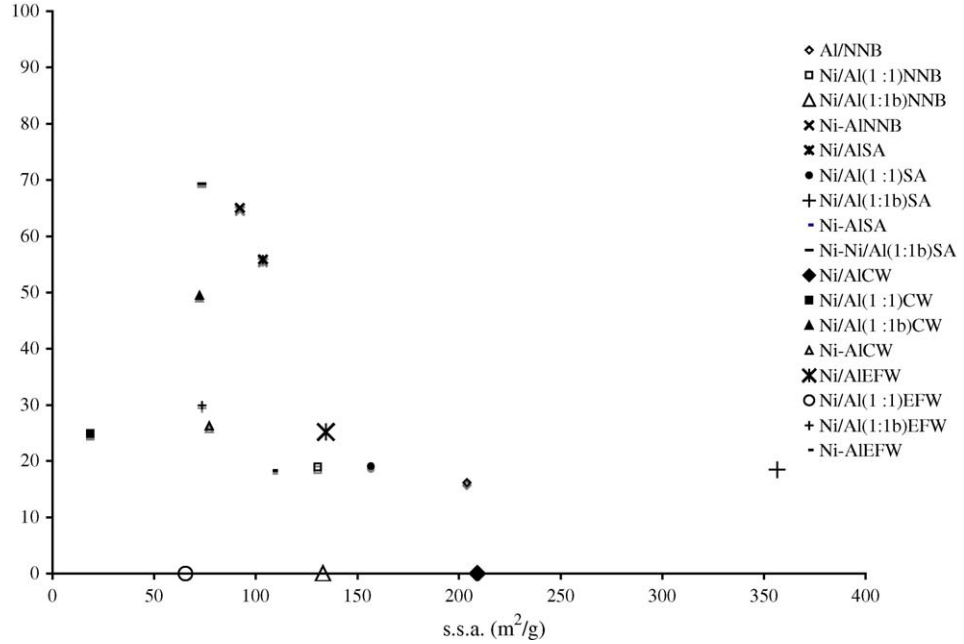

Fig. 19. Dependence of tetralin conversion (T = 450 °C, P = 40 bar) on BET-N_2 surface areas for a series of Ni^{2+} exchanged Al-PILCs. Note the drastic effect of high Ni^{2+} content in pillaring (Ni/Al(1:1) means a molar ratio 1:1 between Ni^{2+} and Al^{3+} in the pillaring solution).

hydrogen and deuterium have scattering lengths of opposite sign, neutrons (unlike X-rays) can both 'see' H atoms and also differentiate between them. For a multiphase material, the scattering density of one phase can be matched with an appropriate H_2O/D_2O mixture and of a second phase by changing water-to-deuterium ratios. The processes of adsorption and fluid penetration in a porous medium may thus be investigated by selecting the scattering length density of the adsorbed phase, ρ_a, to be identical to that of the solid ρ_s. Basically, the value of ρ_a for water is varied by using mixtures of H_2O and D_2O which have scattering length densities of -0.56 and 6.36×10^{10} cm^{-2}, respectively, for the bulk liquids.

This 'contrast matching' technique has permitted developments in SANS structural studies for porous media. For an evacuated solid, the pores have a scattering density ρ_p, which is effectively zero:

$$I(Q) = K(\rho_s - \rho_p)$$

K contains information on the distribution of the size and form of the pores, the nature of the interfacial structure, and the respective volume fraction of the two phases [32].

Fig. 20 shows SANS of EFW before and after pillaring with alumina (Al-EFW) and Mg/alumina (MgAl-EFW, a new PILC) together with contrast-matched SANS. The characteristic feature in PILCs is the presence of well-resolved peaks at high Q values, corresponding to real space lengths between 1.40 and 1.80 Å. Spectra of aluminosilicate-sheet contrast-matched samples (p in the figure) still contain the peak, with that for MgAl-EFW being more pronounced. The peaks completely vanish, however, when the pillars are contrast-matched (inset, left, in Fig. 20) indicating that the corresponding spacing is characteristic of the distance between pillars. Note that the XRPD gives a basal spacing (uncorrected) of 1.73 Å for Al-EFW and 1.87 Å for MgAl-EFW, respectively. The enhanced contrast for MgAl-EFW is due to the presence of the Mg^{2+}, and proves it is indeed in the pillar, as confirmed both by presence of a single peak and similarity of inter-pillar distance with that in Al-EFW.

Table 3
Interpillar distances, w, and fractal dimensions, D_s, for several PILCs [33]

Sample	Qpeak (1/nm)	w (nm)	Ds
EFW	–	–	2.60
Al-EFW	3.59	1.75	2.98
MA-EFW	3.57	1.76	2.99
Al-EFW_p	Weak	–	2.93
MA-EFW_p	3.57	1.76	2.98
Al-EFW_c	–	–	2.53
MA-EFW_c	–	–	2.56
B4	–	–	2.60
Al-B4	4.37	1.44	2.74
FA-B4	3.50	1.80	3.09
	4.22	1.49	

Structural parameters in Table 3 show that there is a considerable difference in interpillar distances between montmorillonite- and beidellite-based PILCs: further that the iron/alumina-pillared Al-B4 has two distinct interpillar distances ascribed to differences in ordering due to different chemical bonds being formed between pillar and sheet on calcination. The table also lists surface fractal dimension, D_s, as determined from log $I(Q)$ versus Q plots. EFW gives $D_s = 2.6$, suggesting a rough, uneven surface (a smooth surface gives $D_s = 2$) which increases on pillaring.

SANS structures of PILCs from synthetic smectites and micas are being analysed to put these emerging structural systematics on a firm basis. However, it should soon be possible (with input from other spectroscopies: FT-IR, MS–NMR, etc.) to correlate SANS with pore size distributions, or indeed correct the latter via the former. Hopefully, this will answer the questions: how many pores are there, what geometry does each pore possess and where exactly in each pore are the catalytically active groups?

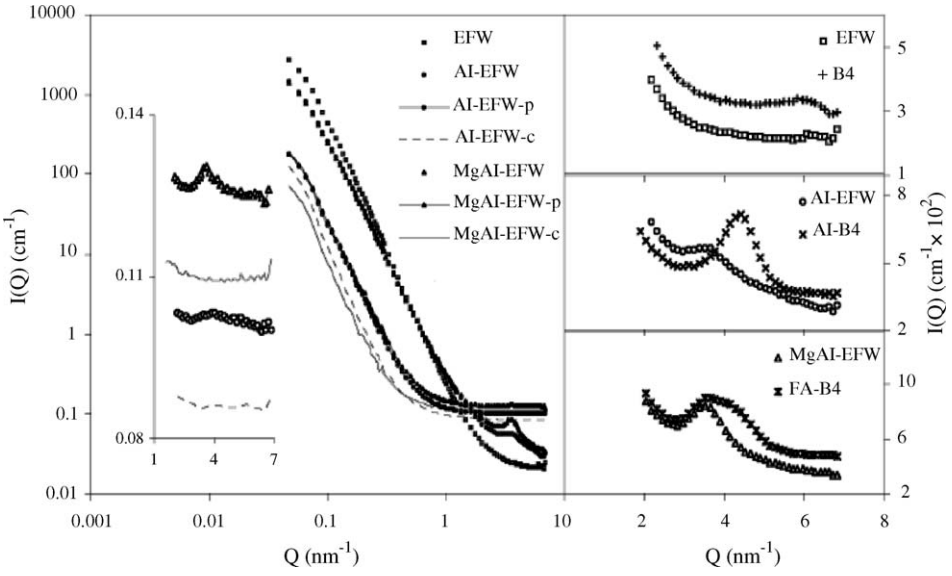

Fig. 20. Small-angle neutron scattering (SANS) of alumina-EFW montmorillonites and -beidellites [32].

Table 4
Structural characteristics of the samples from SANS, XRPD and porosimetry results

Material	$d_{0\,0\,1}$ [a] (nm)	s.s.a.[b] (m^2/g)	D_m [c]	D_s [c]
HMO	1.48	325	–	2.98
Mg-HMO	1.27	70	–	2.60
K10®	–	207	2.53	2.96

[a] From XRPD measurements.
[b] From N_2 isotherms.
[c] From SANS measurements.

11. Some comments on restructured clays

During pillaring via route 1 of Fig. 1, too high a pH of added intercalating polyhydroxy moiety may give rise to some, usually undesired, platelet destruction. Further, clays are often restructured (or 'acid activated') before or after pillaring, to induce yet further porosity and differing active sites. Consequently, the structures of restructured clays – most of which are amorphous and non-amenable to X-ray powder diffraction – are of some importance. The most successful industrially [1] are the K-series prepared *via* HCl-activation at 80–90 °C and Fig. 21 shows the SANS of K10® and those of a new type of (very mildly) restructured montmorillonite H-MO and its magnesium-exchanged derivative.

Analysis provides the results of Table 4, which also lists interlayer distances from XRPD and porosities (see Ref. [34] for details).

K10® has a structure in which the partially destroyed platelets form a triangular stack associated via other platelets into an open rod-like nano-structure. This differs from that suggested in the literature but neatly fits the high surface area and, curiously, is very similar to that suggested for the Zn^{2+} exchanged derivative, the catalyst 'Clayzic' [1].

Instead, it is H-MO which still retains stacking order and the difference appears logical; more heavily destroyed platelets are expected to lead to edge–edge association (see Fig. 22). Conversely, although Mg-HMO also has a rod-like structure, it is composed of parallel-platelets in a nano-particle. This is underlined by the XRPD of Fig. 22 which illustrates how

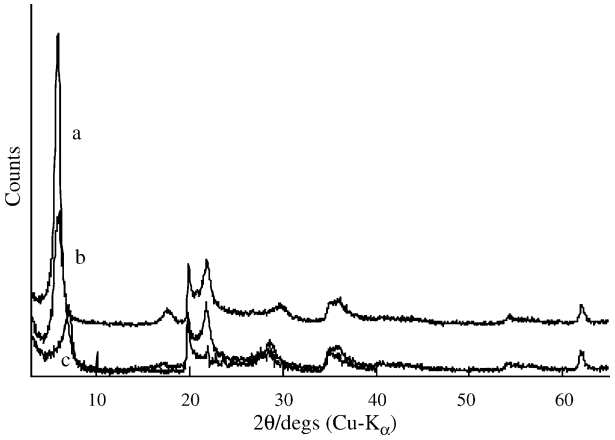

Fig. 22. XRPD of (a) Mg-HMO, (b) H-MO, (c) montmorillonite, illustrating the platelet order enhancement. Note appearance of peak at $d = \ldots$Å, demonstrating that ordering is also higher in (*h k 0*) on restructuring.

re-structuring actually increases platelet ordering, which is enhanced on Mg^{2+} substitution.

Presumably, pillaring of acid-treated clays will give rise to structures similar to K10, whilst pillaring of Mg-HMO should lead to laterally well-ordered PILCs.

This is of some importance because Mg-HMO is an efficient base catalyst for the side-chain alkenylation of *p*-xylene with butene [35] for producing the key organic intermediate naphthalene 2,6-dicarboxylic acid (NDC). NDC is then utilised for–among other things – the production of liquid crystals for LCDs and the high-volume plastic polyethylene naphthenate (PEN). The crucial stage is obtaining 5-(p-tolyl)-2-pentane and 5-(p-tolyl)-2-pentene (PTP) (Schemes 8 and 9):

(Subsequent stages are dehydrocyclisation to 2,6-dimethyl-napthalene followed by oxidation of the Me groups to give NDC, both by standard industrial methods).

Current catalysts, Na-K10® and Cs-exchanged zeolites, operate at >350 °C and provide only low yields (<5%). With butene re-cycling, Mg-HMO as catalyst, instead provides an efficient 2-stage (rather than the current 4-stage) industrial process for arriving at NDC through PTP.

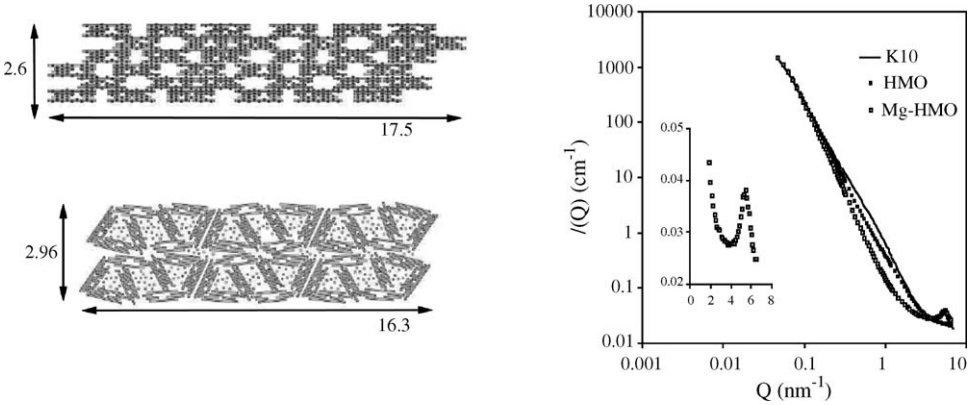

Fig. 21. Right: SANS spectra of K10®, HMO and Mg-HMO. Inset is expansion of the peak in the Mg-clay which gives an Mg^{2+} - Mg^{2+} distance in the HMO interlayer = 1.15 nm; Left: structures of K10® and Mg-HMO.

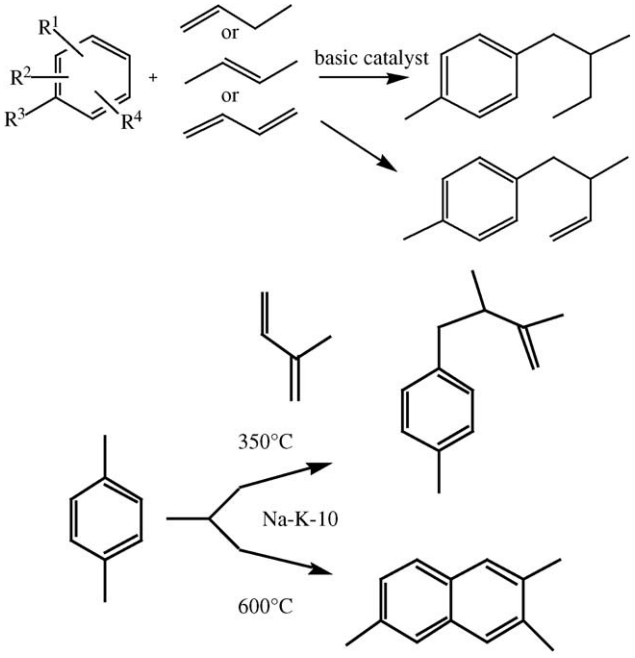

Schemes 8 and 9. Above: new high-yield PTP synthesis. Below: current industrial production of PTP.

To conclude, the major point arising from this brief overview is the importance of standard clays, which can now be prepared (preferably via synthetic clays) and whose structures can be backed up by SANS measurements. Only then can structural variations be applied to naturally derived PILCs and reaction mechanisms established for the different categories of catalytic reactions. This work is underway.

Acknowledgements

The author wishes to thank IKO-Erbslöh GmbH (Germany), Optatech Oy (Finland) and the E.C. (Contracts BRPR-CT97-0545 and G5RD-CT-2000-00272) for financial and moral support.

References

[1] I.V. Mitchell (Ed.), Pillared Layered structures, Current Trends and Applications, Elsevier Applied Science, Amsterdam, 1990;
M.L. Occelli, H.E. Robson (Eds.), Expanded Clays and other Microporous Solids, Academic Press, New York, 1992, p. 229;
For restructured clays:
J.H. Clark (Ed.), Chemistry of Waste Minimisation, Blackie, London, 1995.
[2] C.A.C. Sequeira, M.J. Hudson (Eds.), Multifunctional Mesoporous Materials, NATO ASI Ser., vol. 400, Kluwer Academic, Boston, 1993.
[3] A. Clearfield, M. Kuchenmeister, in: A. Bein (Ed.), Supramolecular Architecture, ACS Symp. Ser., 1989. Vol. 499, p. 129.
[4] J.T. Klopprogge, J. Porous Mater. 5 (1998) 5.
[5] D. Jones, J. Roziere, P. Maireles-Torres, A. Jimenez-Lopez, P. Olivera-Pastor, E. Rodriguez-Castellon, A.A.G. Tomlinson, Inorg. Chem. 34 (1995) 4611.
[6] J.P. Sterte, J. Shabtai, Clays Clay Minerals 36 (1987) 429, for an early example.
[7] E.G.T. Yamaguchi, K. Kitajima, E. Sakai, M. Daimon, J. Ceram. Soc. Japan 111 (2003) 567.
[8] P.T. Tanev, T. Pinnavaia, Science 267 (1995) 865;
see also:
P.T. Tanev, T. Pinnavaia, in: T.J. Pinnavaia, M.F. Thorpe (Eds.), Access in Nanoporous Materials, Plenum, New York and London, 1995, p. 13.
[9] M.S.A. Baksh, R.T. Yang, AIChE J. 38 (1992) 1357.
[10] S. Foglia, A.A.G. Tomlinson, Mol. Cryst. Liq. Cryst. A 311 (1998) 635.
[11] A.A.G. Tomlinson, J. Porous Mater. 5 (1998) 259, and refs. therein.
[12] D. Koch, K. Kesore, A.A.G. Tomlinson, World Patent WO 2004/030817 (to IKO-Erbslöh).
[13] Jellinek, et al. Langmuir 67 (1996) 1162.
[14] A. Gil, G. Guiu, P.A. Grange, M. Montes, J. Phys. Chem. 99 (1995) 301; see also: International Symposium on Charcterisation of Porous Solids, COPS VII, Aix-en-Provence, Proceedings, in press.
[15] H.Y. Zhu, N. Maes, A. Molinard, E.F. Vansant, Microporous Materials 3 (1994) 235.
[16] H.Y. Zhu, G.Q. Lu, N. Maes, E.F. Vansant, J. Chem. Soc. Faraday Trans. 93 (1997) 1417.
[17] A. De Stefanis, Th.A. Steriotis, A.A.G. Tomlinson, J. Phys. Chem., submitted.
[18] Final report, CEA-PLS, Brussels, 1995.
[19] M. Raimondo, A. De Stefanis, G. Perez, A.A.G. Tomlinson, Appl. Catal. A 171 (1998) 85.
[20] A. De Stefanis, G. Perez, A.A.G. Tomlinson, J. Mater. Chem. 7 (1997) 351.
[21] M. Raimondo, G. Perez, A. De Stefanis, A.A.G. Tomlinson, Appl. Catal. A 164 (1997) 119.
[22] M.L. Occelli, Chemtech (1994) 24, and refs. Therein.
[23] P.A. Atkins, in ref. [1].
[24] A. de Stefanis, G. Perez, A.A.G. Tomlinson, Italian patent applied for, 2002.
[25] PLS vs. Zeolites as Sorbents and Catalysts. Part 8. This volume.
[26] K. Bahranowski, J. Janas, T. Machej, E.M. Serwicka, L.A. Vartikian, Clay Miner. 32 (1997) 665.
[27] A. De Stefanis, M. Dondi, G. Perez, A.A.G. Tomlinson, Chemosphere 41 (2000) 1161.
[28] A. De Stefanis, R.C.T. Slade, A.J. Roberts, A.J.Roberts, and A.A.G. Tomlinson, J. Mater. Chem., submitted. A.J. Roberts, Ph.D. Thesis, University of Surrey (UK), 2002.
[29] http://www.bosch.de/start/content/language2/html/734_2739.htm.
[30] A. Corma, V. Gonzalez-Alfaro, A.V. Orchilles, J. Catal. 200 (2001) 34.
[31] C. Cafarelli, B. Pagliari, A. De Stefanis, G. Perez, A.A.G. Tomlinson, J. Mater. Chem, submitted; unpublished results.
[32] A. De Stefanis, A.A.G. Tomlinson, Th.A. Steriotis, K.L. Stefanopoulos, U. Keiderling, Physica B 350 (2004) 521.
[33] Th.A. Steriotis, K.L. Stefanopoulos, U. Keiderling, A. De Stefanis, A.A.G. Tomlinson, Chem. Commun. (2002) 2396.
[34] Th.A. Steriotis, K.L. Stefanopoulos, U. Keiderling, A. De Stefanis, A.A.G. Tomlinson, J. Mater. Chem. 13 (2003) 1145.
[35] A. De Stefanis, G. Perez, A.A.G. Tomlinson, C. Bergström, "Alkylation Process" Int. Patent WO 0155061, 2001 (to Optatech Oy).